Anisotropy of the electron-phonon collision frequency on the Fermi surface of silver*

P. B. Johnson and R. G. Goodrich
Department of Physics and Astronomy, Louisiana State University, Baton Rouge, Louisiana 70893
(Received 23 December 1975; revised manuscript received 7 June 1976)

The anisotropy of the electron-phonon collision frequency on the Fermi surface of silver has been determined from the temperature dependence of radio-frequency-size-effect (RFSE) line amplitudes. In all cases when $\ln A$ is plotted vs T^3 the expected linear relationship is observed. The average collision frequency for 18 parallel field orbits on the Fermi surface was determined from the temperature dependence of the corresponding RFSE signals. Using these average values in an inversion technique, a functional form for the collision frequency over the Fermi surface was determined. Several different functional forms were assumed in order to determine the best fit to the experimental data. In addition the average collision frequency about five tilted field orbits has been determined. These average values are in reasonable agreement with values calculated from the derived analytic expression of the collision frequency.

INTRODUCTION

For many years, the parallel-field radio-frequency size effect (RFSE) has been used as a valuable tool for measuring the caliper values of the Fermi surface of many metals,[1] and for obtaining information about electron-phonon collision frequencies.[2] Experimentally, the RFSE involves the detection of changes in the surface impedance of a thin single-crystal slab of metal placed in a magnetic field applied parallel to the crystal surface. At magnetic field values such that an extremal cyclotron orbit of a carrier exactly spans the sample thickness, an abrupt change in the surface impedance of the sample is observed. The magnitude of the magnetic field at which the change occurs is directly proportional to an extremal dimension of the Fermi surface.

More recently it has been suggested that tilted-field RFSE signals should provide a powerful tool for determining the electron-phonon collision frequency at points on the Fermi surface.[3] These signals occur when the magnetic field is tilted with respect to the sample surface, and the carriers having their velocity parallel to one surface spiral along the field to the opposite sample surface where they again enter the skin depth having their velocity parallel to the surface in an integral number of turns. In the case of tilted-field signals arising from nearly spherical portions of the Fermi surface, however, angles of tilt of the magnetic field out of the plane of the sample from 8° to 15° are usually required to observe signals of sufficient strength to be easily resolved.[4-6] In order to get point-by-point information for the collision frequency on the Fermi surface, one would have to use tilt angles of about 1°. Such angles have proved to be prohibitively small, thus, a new technique to obtain point information was required.

The first attempt to develop such a technique was made by Gantmakher and Gasparov,[7] who determined the anisotropy of the electron-phonon collision frequency $\nu^*(\vec{k})$ on the Fermi surface of copper. Subsequently, Gasparov[8] has used their technique to measure $\nu^*(\vec{k})$ in silver. They used the temperature dependence of the amplitude of parallel-field RFSE signals to calculate the average collision frequency around the orbits giving rise to the parallel-field signals. From the orbit averages of the collision frequencies, an inversion scheme for the data was applied to obtain a functional form for $\nu^*(\vec{k})$. This procedure requires a knowledge of an analytic expression for the Fermi surface $\psi(\vec{k})=0$, and the Fermi velocity distribution. Such information exists for all of the noble metals.[9]

In order to accurately compare the values of $\nu^*(\vec{k})$ measured from parallel-field results to calculations, it is necessary to obtain results from samples much thicker than the electron mean free path. We have devised a method for extrapolating measured results to this limit,[10] and all of the data presented here are obtained from this procedure. In addition, we have measured the temperature dependence of large-angle (~13°) tilted-field RFSE signals, and have determined the average collision frequencies for these orbits. These averages are then compared with the calculated averages, using the function obtained from the inversion process.

THEORY

In the presence of a magnetic field $\vec{H}$, the electrons in a metal move in reciprocal space on the Fermi surface in a plane perpendicular to the direction of $\vec{H}$. Such motion can result in two types of orbits in real space (Fig. 1), which can be observed by means of the RFSE. One type of orbit, Figs. 1(a) and 1(b), arises from extremal dimension trajectories on the Fermi surface, and re-

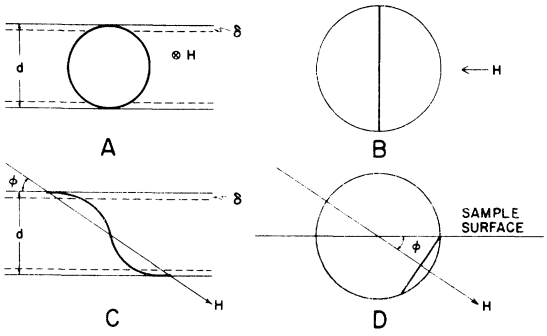

FIG. 1. (a) Electron trajectory on a spherical Fermi surface in real space for the parallel-field RFSE. (b) The orbit corresponding to (a) in k space. (c) Electron trajectory on a spherical Fermi surface in real space for the limiting point tilted-field RFSE. (d) The orbit corresponding to (c) in k space. In all cases, H denotes the magnetic field, d the sample thickness, δ the skin depth, and ϕ the tilt angle.

sults in closed orbits in real space. These extremal orbits will just fit inside of a sample consisting of a thick flat metal crystal of thickness d, when H is parallel to the sample surface, and when $k_c = (e/\hbar c)Hd$, where k_c is an extremal diameter of the Fermi surface, e is the electron charge, $\hbar$ is Planck's constant divided by 2π, and c is the speed of light.[11] Such orbits are called parallel-field extremal orbits. A second type of orbit, Figs. 1(c) and 1(d), results from limiting point trajectories on the Fermi surface, and arises from spiral orbits in real space. An integral number n of complete revolutions of an electron around a spiral orbit will just fit into the sample, provided that it enters the skin depth on each side of the sample with the velocity parallel to the surface. Such an orbit will give rise to a signal if the magnetic field is tilted at an angle ϕ with respect to the sample surface, and $H = 2\pi\hbar K^{-1/2}\sin\phi/ed$, where $K^{-1/2}$ is the Gaussian curvature of the Fermi surface at the limiting point.[12] These orbits are called tilted-field orbits.

The measured amplitude of either type of orbit is governed by the probability that an electron can traverse the sample along an orbit without being scattered.[2] In the case of parallel-field extremal orbits, an electron could possibly make many such traverses without being scattered, in which case

$$A = A_0 \sum_{m=1}^{\infty} \exp\left(\frac{-m\pi\bar{\nu}_{\text{eff}}}{\Omega}\right) = A_0\left[\exp\left(\frac{\pi\bar{\nu}_{\text{eff}}}{\Omega}\right) - 1\right]^{-1}, \tag{1}$$

where $\bar{\nu}_{\text{eff}}$ is the average effective collision frequency for all types of scattering about an orbit, and $\Omega = eH/m^*c$ is the cyclotron frequency, where m^* is the cyclotron mass. In the case where $\pi\bar{\nu}_{\text{eff}}/\Omega \gg 1$, so that an electron will have a high probability of being scattered during half of a cyclotron orbit while traversing the sample only once, $A = A_0\exp(-\pi\bar{\nu}_{\text{eff}}/\Omega)$. For tilted-field orbits, however, the electrons scatter off of the sample surface after making only one traverse of the sample during a complete cyclotron orbit, so in this case $A = A_0\exp(-2\pi\bar{\nu}_{\text{eff}}/\Omega)$ independent of the relationship between $\bar{\nu}_{\text{eff}}$ and Ω.

Unfortunately, parallel-field RFSE measurements cannot always be made on samples which are in the limit where $\pi\bar{\nu}_{\text{eff}}/\Omega \gg 1$. Therefore, a correction must be made for multiple orbit effects.[10] To make this correction, one must consider the total effective scattering frequency, $\bar{\nu}_{\text{eff}} = \bar{\nu}_I + \bar{\nu}_P(T)$, where $\bar{\nu}_I$ is the temperature-independent collision frequency of electrons with static impurities, and $\bar{\nu}_P(T)$ is the temperature-dependent collision frequency of electrons with phonons. For the orbits we are considering, it is observed that plots of $\ln A$ vs T^3 yield straight lines, and so $\bar{\nu}_P = CT^3$, where C is a constant for a particular orbit and a particular sample thickness. (The reasons for, and the implications of the observed T^3 behavior will be discussed below.) Substituting for $\bar{\nu}_{\text{eff}}$ in Eq. (1), we obtain

$$\ln A = \ln A_0 - (\pi/\Omega)CT^3 - (\pi/\Omega)\bar{\nu}_I - \ln(1 - e^{-\pi\bar{\nu}_{\text{eff}}/\Omega}) . \tag{2}$$

For the orbits and temperature range we are considering, $\pi\bar{\nu}_I/\Omega$ is on the order of one and $\pi CT^3/\Omega \ll 1$. Under these conditions, Eq. (2) becomes[10]

$$\ln(A/A_0) = C_1 + (\pi/\Omega)C_2T^3 ,$$

where

$$C_1 = -(\pi\bar{\nu}_I/\Omega) - \ln(1 - e^{-\pi\bar{\nu}_I/\Omega})$$

and

$$C_2 = C/(1 - e^{-\pi\bar{\nu}_I/\Omega}) .$$

Therefore, the slope s of a $\ln A$-vs-T^3 plot is $s = (\pi/\Omega)C_2$, yielding

$$\pi/\Omega s = (1/C)(1 - e^{-\pi\bar{\nu}_I/\Omega}) .$$

Finally, substituting $\Omega = eH/m^*c$ and $H = k_c\hbar c/ed$ for each observed orbit, we obtain

$$\frac{d}{s} = \frac{k_c\hbar}{\pi m^* C}(1 - e^{-(\pi m^*/k_c\hbar)\bar{\nu}_I d}) . \tag{3}$$

If a value of $\bar{\nu}_I$ can be obtained, Eq. (3) can be used to extrapolate values of C, the electron-phonon scattering rate in a sample in which multiple electron orbits can be completely neglected (i.e., $\pi\bar{\nu}_{\text{eff}}/\Omega \gg 1$). The values of C will be the true value of the collision frequency around the corresponding orbits on the Fermi surface.

In order to obtain values of $\bar{\nu}_I$, values of d/s must be obtained as a function of d, and Eq. (3) must be fit to these values. Such a procedure need only be used on one orbit if $\bar{\nu}_I$ is isotropic. Anisotropies in $\bar{\nu}_I$ can be found by applying the analysis to several orbits widely spaced on the Fermi surface.

Using the extrapolated values of $C = \bar{\nu}_P/T^3$ for parallel-field extremal orbits, one would like to be able to calculate a functional form for the electron-phonon collision frequency $\nu^*(\vec{k})/T^3$ over the Fermi surface. Such a function can be obtained using the procedure devised by Gantmakher and Gasparov.[7] In this case,

$$\bar{\nu}_{P_j} = \frac{\hbar}{2\pi m_j^*} \oint \frac{\nu^*}{V_\perp} dk \ ,$$

where j denotes an extremal orbit, and $V_\perp$ is the projection of the Fermi velocity onto the plane of the orbit. If one measures values of C_j for a series of extremal orbits and assumes a functional form for $\nu^*(\vec{k})$ containing adjustable parameters, then using the integral relationship stated above, the parameters can be determined. Once an analytical expression for ν^* has been obtained in this manner, it can be used to compute the average collision frequency for any electron trajectory.

The RFSE imposes boundary conditions on the electron orbits which could affect the scattering efficiency at different points on the orbits. Gantmakher and Gasparov[7] have used a factor of $|\cos\gamma|$, where γ is the angle between the electron velocity and the sample surface, to account for the scattering efficiency. Gasparov later described in detail the geometrical conditions under which one should use this correction. We will show that while the effects described by these authors can be present, they must lead to a temperature dependence other than the T^3 dependence we have observed.

The T^3 dependence of the scattering frequency or mean-free path arises in the following manner. In general, there are three factors that enter into determining the temperature-dependent mean-free path of an electron in a metal.[13] First there is the number of phonons available to cause the scattering, and because the electrons are confined to the Fermi surface and the temperature is low, this number is proportional to T^2. Second, the square of the matrix element for the interaction is proportional to the magnitude of the phonon wave vector q, and this leads to an additional T dependence. These two factors give the T^3 law, and it is explicitly assumed that all scattering events are effective. If there is any angular dependence to the effectiveness, then the T^3 law must be altered. For example, to obtain the resistivity, one must multiply by a factor of $(1 - \cos\theta)$, where θ is the average angle through which the electron velocity direction is changed. At low temperatures, this leads to a T^5 law. Thus, one concludes that if all scattering events are effective, $\bar{\nu}_P$ should be proportional to T^3.

In the RFSE one must consider the effect of averaging the collision frequency along the extremal orbit to account for different scattering efficiencies caused by the presence of the skin depth and the location of the sample surfaces relative to the orbit center.[2,7,8] Gasparov and Gantmakher[8] have given geometrical arguments for the experimental conditions under which these effects would be appreciable, and Wagner and Albers[14] have made detailed calculations of the effect of small-angle scattering. If one considers a circular orbit of radius R, then the effect of a scattering event due to a phonon of average wave-vector q, which causes a change in an electron's velocity direction by an angle θ is illustrated in Fig. 2(a). When this event occurs, the center of the electron orbit is shifted by a distance d. The angle γ in Fig. 2 differs only from the angle between the direction of the electron velocity and $\hat{n}$ by θ. Since θ is very small at all temperatures of interest, γ is used to mean either angle.

As scattering through the angle θ occurs at various points on the real space orbit, the locus of new orbit centers defines a circle of radius d. As can be seen from Fig. 2(a), the shift in the orbit center is given by $d = R(q/k_f)$. If the scattering event is to be effective in removing the electron from the signal, then the orbit center must be shifted toward the surface of the sample (in the z direction) by an amount greater than the skin depth δ. This gives rise to the effectiveness condition $\Delta z > \delta$, given by Gasparov and Gantmakher.[8] Since $\Delta z = d\cos\gamma$, the condition for effective scattering is $d\cos\gamma > \delta$, or $R(q/k_F)\cos\gamma > \delta$. This condition can only be satisfied when there is some value of γ such that $\cos\gamma > \delta/d$. In Fig. 2(b), this value of γ, γ_{max}, defines the boundary between the shaded (ineffective) and unshaded (effective) region of shifted orbit center positions. The boundary between ineffective and effective scattering positions on the orbit is defined by

$$\cos\gamma_{max} = (\delta/R)\, k_F/q \ .$$

The average value of q in this equation is temperature dependent. Thus, for different temperatures, a different number of electrons are effectively scattered. The ratio of the number of effective scattering events to the total number of scattering events is proportional to the unshaded area of Fig. 2(b). Thus, one concludes that if a geometrical effectiveness weighting factor is to be used

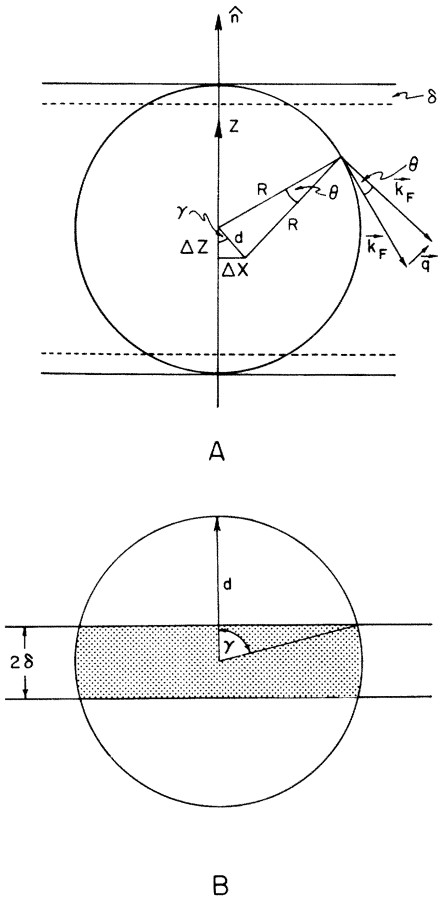

FIG. 2. (a) Result of a scattering event on a circular orbit in the RFSE geometry, where γ is the angle between the orbit center displacement and $\hat{n}$. (b) Locii of orbit centers produced by scatterings shown in (a) at different points on the orbit. The thickness of the shaded area is twice the skin depth, and the radius d is determined by the average scattering angle θ.

in the analysis of data, it should only be necessary when the strongest temperature dependence of that factor occurs, and the data does not exhibit a T^3 behavior. We have not been able to detect any deviation from T^3 behavior for any of our data, therefore, no geometrical effectiveness factor has been used in the analysis. Gasparov and Gantmakher[7,8] used an effectiveness factor in analyzing Cu, but not in analyzing Ag. Since all of their data appears to exhibit a T^3 dependence, we conclude that it should not have been used in either case.

EXPERIMENTAL CONSIDERATIONS

Sample preparation

The experiments were performed on thin single-crystal samples of silver which were spark cut from a large oxygen-annealed crystal having a resistance ratio of about 7000. Slabs 2 cm in diameter were cut to a thickness of 3 mm, and then thinned using an acid polishing technique similar to that described by Young and Wilson.[15] Slightly more than 1 mm of material was removed from each side of the sample during polishing, thus insuring that the spark damage resulting from the cutting was completely removed. The samples were polished using a mixture of H_3PO_4, CH_3COOH, and HNO_3, in a ratio of 55:25:20. The resulting surfaces had a mirrorlike finish, and no strain could be detected from x-ray photographs. Two samples were produced. One sample had a [001] normal, and was 0.201 mm thick, while the other sample had a [110] normal, and was 0.238 mm thick. In addition, a second [110] normal sample was cut. This sample was thinned in stages. From it we measured values of d/s vs d, in order to obtain the values of $\bar{\nu}_I$ necessary for the extrapolation of the data obtained from the other two samples.

Apparatus

The sample was placed in the tank coil of a 5-MHz limiting oscillator.[16] This coil consists of about 30 turns of No. 27 wire, and was free standing after being cast in Duco cement. The oscillator was part of a standard field modulation RFSE detection system,[11] using a modulating frequency of 25 Hz. The amplitude of the RFSE signals was measured from plots of dR/dH versus either magnetic field or tilt angle, depending on whether parallel-field or tilted-field measurements were being performed. The sample coil and dewar system were located in the gap of a 12-in.-diam pole-face iron-core magnet which provided a horizontal magnetic field in the plane of the sample. The sample normal $\hat{n}$ is vertical in this arrangement, and the magnitude of the horizontal field can be swept as is necessary for parallel-field measurements. In this system, the direction of the overall magnetic field can be tilted out of the plane of the sample by changing the current in a vertical solenoid surrounding the bottom of the dewar system. To observe tilted-field signals, the horizontal field was held constant and the vertical field in the solenoid was swept. Thus, the resultant field in the sample rotates out of the plane of the sample. For small tilt angles, such a system effectively sweeps the angle, requiring only a small correction for the change in magnitude of the field. This system is very convenient, since the orientation of the direction of the field with respect to the crystal axes can be changed between sweeps by simply rotating the magnet producing the horizontal field about a vertical axis.

The temperature of the sample was controlled between 1.2 and 7 °K by a stainless-steel double-wall vacuum-can system which isolated the sample from the liquid-helium bath. The inner can, which contained an exchange gas, was heated above the temperature of the 1.2 °K bath by means of a heating element attached to the can. The temperature inside the inner can was monitored using a calibrated carbon resistor. Using this system, it was possible to hold the temperature inside of the can constant for an indefinite period of time.

EXPERIMENTAL RESULTS

Parallel-field orbits

Values of d/s vs d were measured for two parallel-field orbits in the $\hat{n} \| [110]$ samples at sample thicknesses of 0.238, 0.43, and 0.59 mm (Fig. 3). At 0.7 mm, the amplitude of the observed signals was too small to measure accurately, and at 0.8 mm, no signals were observed. The orbits were observed when the magnetic field was oriented at 5° and 55° from the [100] direction. We fitted Eq. (3) to this data, and obtained the best fit in each case with a value of $\bar{\nu}_I = 3 \times 10^9$ sec^{-1}. Since the two orbits yielded identical values of $\bar{\nu}_I$, we have assumed that $\bar{\nu}_I$ is isotropic and have used this value of $\bar{\nu}_I$ to correct all of our data.

Eighteen parallel-field central belly-orbit signals were observed in the $\hat{n} \| [001]$ and $\hat{n} \| [110]$ samples by rotating the horizontal magnetic field in 5° increments (Table I, Fig. 4). The orientation of the symmetry axes in the sample with respect to the magnetic field direction was determined to within 0.5° from the symmetry of the field position of the RFSE lines. Using the relation $k_c = (e/\hbar c)Hd$, we determined the sample thickness from the known caliper values k_c of the Fermi surface,[9,17] along with the measured magnetic field values for the belly orbit signals when the field was parallel to one of the [100] axes. For the belly-orbit signal in the $\hat{n} \| [001]$ sample, $k_c = 2.52 \times 10^8$ cm^{-1} and $H = 824$ G, and in the $\hat{n} \| [110]$ sample, $k_c = 2.31 \times 10^8$ cm^{-1} and $H = 640$ G. The resulting thicknesses are 0.201 and 0.238 mm, respectively. These thicknesses agree within our measuring accuracy 1%, with values obtained by weighing and measuring the surface area.[11] Using these thicknesses, the calipers for the other 16 orbits were calculated and compared with the appropriate

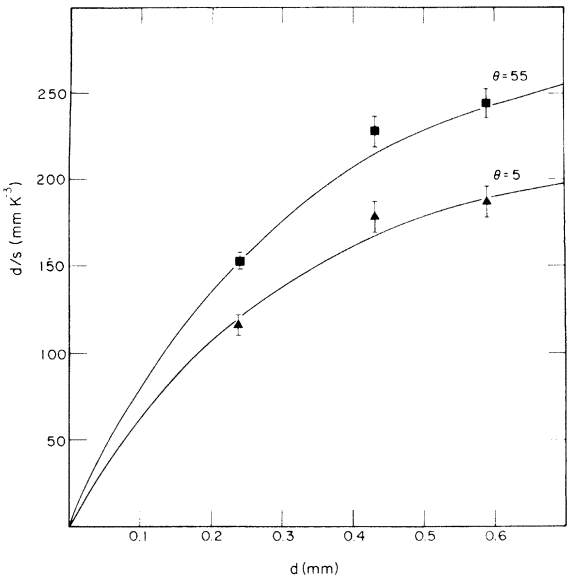

FIG. 3. Measured values of d/s vs d in $\hat{n} \| [110]$ samples. The squares and triangles represent data taken with the magnetic field oriented at $\theta = 55$ and $\theta = 5$, respectively. The curves are the best fit to the data using Eq. (3). $\bar{\nu}_I = 3 \times 10^9$ sec^{-1} for each curve. $C = 3.29 \times 10^6$ sec^{-1} for the $\theta = 55$ curve and $C = 4.16 \times 10^6$ sec^{-1} for the $\theta = 5$ curve.

TABLE I. Values of θ, the angle of the magnetic field measured from [100]; m^*, the cyclotron mass in units of the electron mass, and extrapolated values $\bar{\nu}_P/T^3$ in units of 10^6 sec^{-1} °K^{-3} for each of our measured orbits in the [001] and [110] samples. $\bar{\nu}_P'/T^3$ are Gasparov's values for the same orbits.

	$\hat{n} \| [001]$ sample				$\hat{n} \| [110]$ sample			
No.	θ	m^*	$\bar{\nu}_P/T^3$	$\bar{\nu}_P'/T^3$	No.	θ	m^*	$\bar{\nu}_P/T^3$	$\bar{\nu}_P'/T^3$
1	0°	0.930	3.92	5.9	9	0°	0.940	4.23	5.9
2	5°	0.930	3.15	5.5	10	5°	0.939	4.29	5.9
3	10°	0.932	2.28	5.4	11	10°	0.937	4.31	6.1
4	15°	0.935	3.18	5.4	12	15°	0.930	4.23	6.2
5	20°	0.947	5.22	6.1	13	20°	0.938	4.64	6.4
6	25°	0.962	6.84	8.1	14	50°	0.944	3.36	4.9
7	30°	1.027	8.28	10.5	15	55°	0.940	3.28	4.8
8	35°	1.180	18.06	···	16	60°	0.950	4.85	6.0
					17	65°	0.985	6.66	7.9
					18	70°	1.025	8.35	11.0

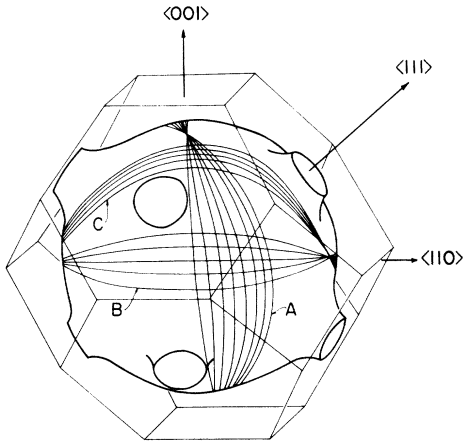

FIG. 4. Location of measured parallel-field RFSE orbits on the Fermi surface of silver. Group A corresponds to orbits 1–8, B to orbits 9–13, and C to orbits 14–18 listed in Table I.

values of the Fermi diameter calculated by Halse.[9] The agreement was good to within 0.3%.

The amplitude of each of the 18 orbits was measured as a function of temperature from 1.2 to 6 °K, and in all cases the linear relationship of $\ln A$ vs T^3 was observed. The slopes of the plots were determined by the least-squares method, and the coefficient of determination for each plot was at least 0.99. Using these values for the slopes, along with the measured magnetic field values and the experimental cyclotron masses m^*, as determined by Howard,[18] we extrapolated values of $C = \bar{\nu}_P/T^3$ for each orbit (Table I). In addition, we measured the amplitude of signals arising at twice the field of the primary signal. Such double field signals correspond to orbits of half the diameter of the primary orbit, and therefore, it takes two orbits to span the sample. The temperature dependence of the amplitude of the double field signal was identical to that of the primary signal.

Tilted-field orbits

Five tilted field RFSE signals were measured in the $\hat{n} \| [001]$ sample by tilting the magnetic field with the solenoid (Table II). Each signal corresponds to a particular horizontal field between $\theta = 25°$ and 45°, in 5° increments, where θ is measured from the [100] axis. For the $\hat{n} \| [001]$ sample, the expression $H = 2\pi n \hbar K^{-1/2} \sin\phi/ed$ yields $H = 2971 \sin\phi$ if $n = 1$ and if $K^{-1/2}$ is assumed to be the free electron Fermi radius. With the horizontal field fixed at 550 G, the $n = 1$ signal is expected to occur when the vertical field in the solenoid is at 129 G (Fig. 5). The resultant field is 565 G, and the tilt angle ϕ is 13.22°. The position on the signal corresponding to these values occurs slightly toward the small tilt-angle side (Fig. 5). It has been thought that the small-angle side of the signal should correspond to orbits which just reach from the skin depth near one surface to the skin depth near the other, while the large-angle side of the signal corresponds to orbits going from one sample surface to the other. In this case, the large-angle side of the signal should correspond to the predicted tilt angle.[4] However, assuming a value for the skin depth which is about 10 times larger than expected, we can, at most, expect the signals to be 0.5° wide instead of the measured 4°. Therefore, the standard argument does not apply, and there seems to be no reason to favor the large-angle side of the signal as corresponding to the calculated tilt angle. We are unable to account quantitatively for the 4° width of the signal, but it seems to be standard for tilted-field signals aris-

TABLE II. Values of θ, the angle of the horizontal magnetic field measured from [100]; $m^* = \hbar/2\pi m_e) \oint (1/V_\perp)\, dk$; $\bar{\nu}_P/T^3$, the experimental value for the collision frequency in units of 10^6 sec^{-1}°K^{-3}, and $\bar{\nu}_P'/T^3 = (\hbar/2\pi m^*) \oint (\nu^*/V_\perp)\, dk$ for each tilted-field orbit.

	$\hat{n} \| [001]$ sample		$\phi = 13.22°$	
No.	θ	m^*	$\bar{\nu}_P/T^3$	$\bar{\nu}_P'/T^3$
1	25°	1.321	10.69	9.20
2	30°	1.119	10.37	8.70
3	35°	0.997	12.46	7.51
4	40°	0.935	7.23	6.37
5	45°	0.918	9.53	5.84

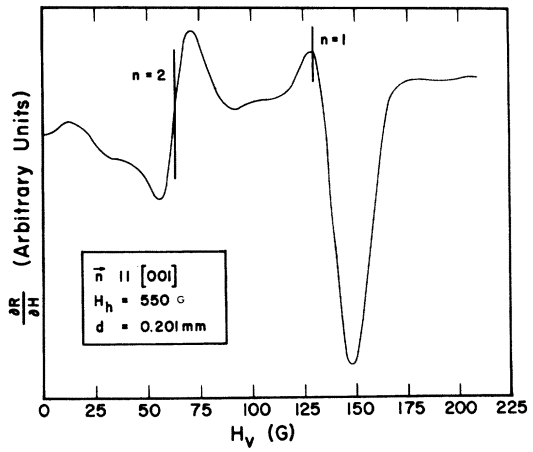

FIG. 5. Example of a limiting point tilted-field RFSE signal. dR/dH is plotted vs the vertical magnetic field in the solenoid. $n = 1$ and $n = 2$ denote the points on the line corresponding to where the one revolution and two revolution spiral orbits are expected to occur. The horizontal magnetic field H_h is parallel to [100].

ing from spherical regions on the Fermi surface.[4–6]

The temperature dependence of the amplitude was measured for each signal, and the resulting plots of $\ln A$ vs T^3 yielded straight lines (Fig. 6), the slopes of which were calculated by a similar technique and with an equivalent error to that described in the parallel-field case. Using the expression $\bar{\nu}_P = (\Omega/2\pi)\ln(A_0/A)$, values of $\bar{\nu}_P/T^3$ were calculated from the slope, the value of H, and the value of m^* for each orbit (Table II). In this case, however, the values of m^* were calculated from Halse's[8] analytic expression for the Fermi velocity by numerically evaluating the integral $m^* = (\hbar/2\pi) \times \oint (1/V_\perp)\, dk$, where the integral is performed around the particular tilted-field orbit. It should be remembered that in tilted-field orbits, multiple orbit effects can be neglected since the electron can complete only one orbit before being scattered.

ANALYSIS

Parallel-field data

Using the extrapolated values of $\bar{\nu}_P/T^3$ for each orbit, a functional form for $\nu^*(\vec{k})$ can be calculated following the procedure outlined by Gantmakher and Gasparov.[7] Assuming $\nu^*(\vec{k})$ is of the form $\nu^*(\vec{k}) = T^3 \sum_{i=1}^{t} \omega_i F_i(\vec{k})$, and substituting into the integral expression

$$\bar{\nu}_{P_j} = \frac{\hbar}{2\pi m_j^*} \oint_j \left(\frac{\nu^*(\vec{k})}{V_\perp} \right) dk \ ,$$

one obtains

$$\frac{\bar{\nu}_{P_j}}{T^3} = \sum_{i=1}^{t} a_{ij}\omega_i, \quad j = 1, 2, \ldots, p \ ,$$

in which

$$a_{ij} = \frac{\hbar}{2\pi m_j^*} \oint \frac{F_i(\vec{k})}{V_\perp(\vec{k})} dk \ ,$$

where

$$V_\perp(\vec{k}) = V(\vec{k})[1 - (\vec{\nabla}\psi \cdot \vec{B}/|\vec{\nabla}\psi||\vec{B}|)^2]^{1/2} \ ;$$

the line integral is around the jth orbit on the Fermi surface given by $\psi(\vec{k}) = 0$,[9] and p is the number of measured orbits. In general, $t < p$, yielding an overdetermined set of equations whose best set of coefficients, ω_i, can be determined by minimizing the Euclidean norms.

As an initial guess for $F_i(\vec{k})$, we used the first terms of the symmetrized Fourier series expansion[19]

$$F_{lmn}(\vec{k}) = \sum \cos\left(\frac{lak_x}{2}\right) \cos\left(\frac{mak_y}{2}\right) \cos\left(\frac{nak_z}{2}\right),$$

($l^2 + m^2 + n^2 = 0, 2, 4, \ldots$ for an fcc lattice, $a = 4.0692$ Å, and the sum denotes the permutation of $x\ y\ z$) and determined the best fit for from three to eight terms of the series. The best four-term fit (Fig. 7) is

$$\nu^*/T^3 = (-99.28 - 306.0F_{110} - 39.93F_{200} - 2.703F_{211})\ (10^6\ \text{sec}^{-1}\,^\circ\text{K}^{-3}), \tag{4}$$

and has a root-mean-square error of 16%. The large error is mostly due to orbits Nos. 8 and 18 in Table I. These two orbits go far up onto the neck and as a result have large values of $\bar{\nu}_P/T^3$. If this four-term fit is redone without including these two orbits in the data (Fig. 7), the rms error decreases to 13.5% and we obtain

$$\nu^*/T^3 = (-54.56 - 166.5F_{110} - 24.46F_{200} - 10.05F_{211})\ (10^6\ \text{sec}^{-1}\,^\circ\text{K}^{-3}) \ . \tag{5}$$

As can be seen in Fig. 7, the maximum near ⟨010⟩ has decreased, and the increase in the vicinity of the neck is not so rapid in the curve resulting from the 16-orbit fit compared to the curve resulting from the 18-orbit fit. Apparently, by including orbits Nos. 8 and 18, the accuracy in the vicinity of the neck is increased, while the accuracy near

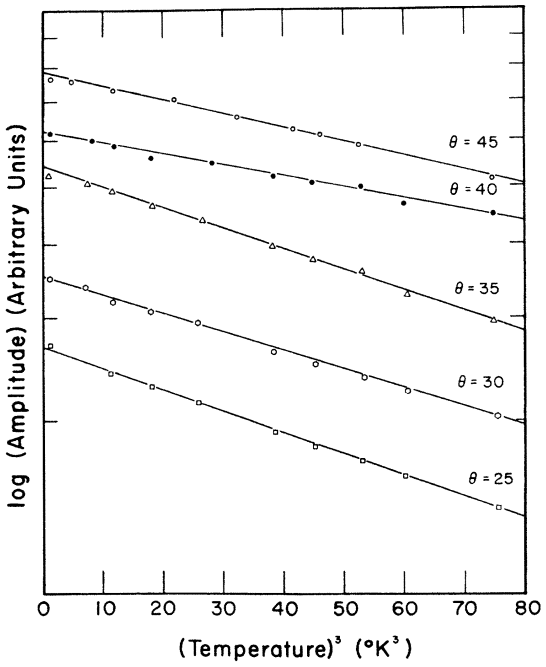

FIG. 6. Log (amplitude) vs (temperature)^3 for each of the measured tilted-field orbits in the [001] sample. θ is the orientation of the horizontal magnetic field measured from [100].

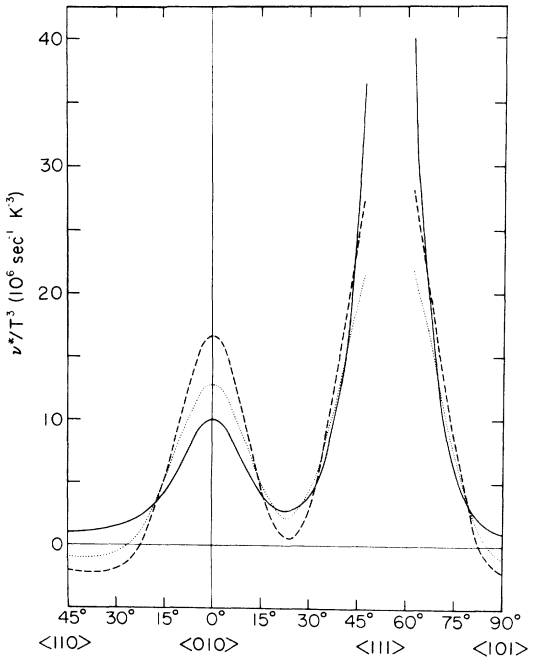

FIG. 7. Anisotropy of ν^*/T^3 along symmetry lines of silver. The dashed curve corresponds to Eq. (4), the dotted curve to Eq. (5), and the solid curve to Eq. (6).

⟨010⟩ is decreased. The problem in fitting data near the neck arises from the fact that the function is forced to become much larger in the vicinity of the neck than elsewhere. In order to overcome this difficulty, we have developed a slightly different procedure. Previous work on copper[7] and silver[8] has shown that the anisotropy in $\nu^*(\vec{k})$, in general, follows the anisotropy of the Fermi radius.[20] Thus, we have multiplied each $F_i(\vec{k})$ by the dimensionless quantity $(|\vec{k}| - k_{\min})/k_{\min}$, where $k_{\min}$ is selected to be some number that is less than $|\vec{k}|$, the Fermi radius, for all $\vec{k}$ on the Fermi surface. This expression forces the expansion to be large near ⟨010⟩, and larger yet near ⟨111⟩. We have treated $k_{\min}$ as a variable quantity and retained the first three terms so that we effectively still have a four-term fit. By adjusting $k_{\min}$ to be 1.148 72 $\times 10^8$ cm^{-1}, we obtained the following function (Fig. 7):

$$\nu^*/T^3 = (-379.1 - 1416F_{110} - 201.6F_{200}) \times [(|\vec{k}| - k_{\min})/k_{\min}]\, 10^6 \text{ sec}^{-1}\,^\circ\text{K}^{-3}\,, \qquad (6)$$

which has an rms error of 13%. This error is slightly smaller than the error obtained in the four term fit without the orbits near the neck (Eq. 5); however, in determining the coefficients for Eq. (6), we have included all 18 orbits. As can be seen in Fig. 7, this fit retains the accuracy of the 16-orbit fit [Eq. (5)] near ⟨010⟩, and even improves on the 18-orbit [Eq. (4)] fit near the neck. In addition, Eq. (6) has the pleasing property of being positive everywhere, and therefore always yielding a physical solution.

By increasing the number of terms beyond four in any of the fits, the function $\nu^*(\vec{k})$ starts to oscillate. An example of this behavior is shown in Fig. 8, where the results for three, six, seven, and eight-term fits to 18 orbits using only a symmetrized Fourier series expansion are shown. The three-term fit has the same anisotropy as the four-term fit (Fig. 7), and is only slightly different in magnitude with a slightly larger error. The error in the six-term fit is 21%, the seven-term fit is 14%, and the eight-term fit is 13.5%; however, both the six and eight-term fits oscillated between ⟨110⟩ and ⟨010⟩. Although the seven-term fit is smooth and has about the same magnitude as our best fit [Eq. (6)] near ⟨010⟩, it is negative near ⟨110⟩ and therefore cannot be correct in this region.

A similar investigation of the effects of increasing the number of terms in the fit has been done for the symmetrized Fourier series expansion 16-orbit fit. In this case we do not include the two orbits which contribute to the large increase in the region of the neck, and as a result, the increase in the magnitude of the oscillations with increasing number of terms is not so great. We have also redone the Gantmakher and Gasparov fit[7] to their copper data. This data is for orbits which include even less

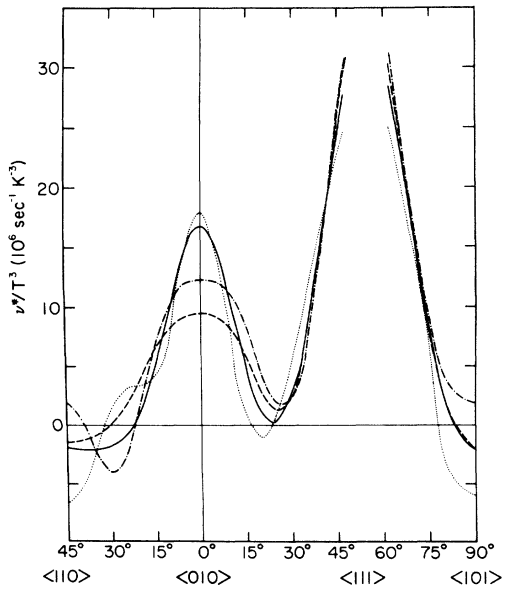

FIG. 8. Anisotropy of ν^*/T^3 along symmetry lines of silver. The solid curve shows the results of including three terms in the fit, the dotted curve includes six terms, the dashed curve includes seven terms, and the dash-dot curve includes eight terms.

emphasis on the neck region, and in this case the oscillations are smaller still, but (as they point out) four terms correspond to the most reasonable fit.

A similar determination of $\nu^*(\vec{k})$ in silver has recently been reported by Gasparov.[8] He also used values of $\bar{\nu}_P/T^3$, determined from the temperature dependence of parallel-field RFSE signals, and fit his data to a five-term symmetrized Fourier series expansion. As can be seen in Table I, his measured values of $\bar{\nu}_P/T^3$ are all larger than ours. Because he did not account for multiple electron orbits within his samples, we would expect his values to be larger if his measurements were not made in the limit where $\pi\bar{\nu}_{\text{eff}}/\Omega \gg 1$. As can be seen in Fig. 3, the values of d/s increase with thickness, and therefore, $\bar{\nu}_P/T^3$ should decrease as we approach the asymptotic value corresponding to the conditions where $\pi\bar{\nu}_{\text{eff}}/\Omega \gg 1$. It should be noted that his data on the $\hat{n} \parallel [110]$ sample show approximately the same anisotropy as ours; however, his data on the $\hat{n} \parallel [001]$ sample do not. Our values of $\bar{\nu}_P/T^3$ from $\theta = 0°$ to $\theta = 15°$ show a larger anisotropy than his. It is possible that the anisotropy difference is a result of our data having been taken on a thin sample. We observed the line shape of the signals to be more resolved in thin $\hat{n} \parallel [001]$ samples. The problem occurs because the parallel-field belly orbit signal overlaps another signal, due to open orbits. The belly orbit and open orbit signals merge together as the sample thickness is increased. In fact, the caliper values computed from the field positions of our signals agree exactly with Halse's[9] calipers, while Gasparov had to refit Halse's expression for the Fermi radius to obtain agreement with his caliper data.

Tilted-field data

Using our Eq. (6), we can calculate the average collision frequency about each of our measured tilted-field orbits by evaluating the integral

$$\bar{\nu}_P = \frac{\hbar}{2\pi m^*} \oint \frac{\nu^*(\vec{k})}{V_\perp} dk \ ,$$

where $\nu^*(\vec{k})$ is given by Eq. (6). These results are listed in Table II, and as can be seen, are in reasonably good agreement with the experimental values. In a similar investigation of tilted-field orbits on the Fermi surface of copper,[21] our experimental values were about 3.5 times larger than the values calculated using Gantmakher and Gasparov's[7] expression for $\nu^*(\vec{k})/T^3$. The reason for the discrepancy in this case is probably due to the fact that their data did not include orbits which extended far up onto the necks. Therefore, their expression for $\nu^*(\vec{k})$ is not accurate in the neck region of the Fermi surface over which the measured tilted field orbits ran. In the case of silver orbits, Nos. 8 and 18 in Table I went up onto the neck, and this data was included in our best fit (Eq. 6). This fit has the additional factor $(|\vec{k}| - k_{\text{min}})k_{\text{min}}$, which greatly improves the fit in the neck region. The good agreement between the measured and calculated average collision frequencies of the tilted-field orbits reflects the accuracy of this fit to the parallel-field data, as opposed to fits obtained from a straight symmetrized Fourier series expansion. When tilted-field orbit average scattering frequencies are computed using the straight symmetrized Fourier series best fit [Eq. (5)], discrepancies with experimental values are found for Ag similar to the ones found in Cu.

SUMMARY

We have observed the temperature dependence of the amplitude for 18 parallel-field extremal orbits and five tilted-field orbits on the Fermi surface of silver. In all cases, plots of $\ln A$ vs T^3 demonstrated the expected linear relationship, and from the slopes of the graphs, the average electron-phonon collision frequency $\bar{\nu}_P/T^3$ was determined for each orbit. Using the extrapolated values determined from the parallel-field data, a functional form for the anisotropic $e-p$ scattering frequency, $\nu^*(\vec{k})$ was derived which fits the data with an rms error of 13%. This function uses a combination of the first terms of a symmetrized Fourier series expansion and an empirical factor which increases the anisotropy in both the vicinity of the neck and near $\langle 010 \rangle$. The factor we have introduced is $(|\vec{k}| - k_{\text{min}})/k_{\text{min}}$, and it multiplies each of the expansion terms. This factor helps to distort $\nu^*(\vec{k})$ to insure a more accurate fit over all regions of the Fermi surface, including the neck. Using this improved fit, we have calculated the average collision frequency for each of the tilted-field orbits, and compared them with the measured values. In all cases, the calculated values were in good agreement with the measured values.

ACKNOWLEDGMENTS

One of the authors (R.G.G.) would like to thank the Scientific Research Council of Great Britain for its support during the initial phases of this work, and Professor R. G. Chambers, Dr. Derek Parsons, and the low-temperature group at the H. H. Wills Physics Laboratory for their hospitality during his stay there. Many helpful discussions were also held with Professor C. G. Grenier and Dr. J. C. Kimball.

*Work supported in part by the NSF Grant No. DMR73-02427.

[1]P. B. Visscher and L. M. Falicov, Phys. Status Solidi 54, 9 (1972).
[2]V. F. Gantmakher, Rep. Prog. Phys. 37, 317 (1974).
[3]R. G. Chambers, Phys. Kondens. Mater. 9, 171 (1969).
[4]T. G. Blaney and D. Parsons, J. Phys. C 3, 126 (1970).
[5]A. Myers, S. G. Porter, and R. S. Thompson, J. Phys. F 2, 24 (1972).
[6]D. K. Wagner, R. C. Albers, and M. Roy, Solid State Commun. 15, 1337 (1974).
[7]V. F. Gantmakher and V. A. Gasparov, Zh. Eksp. Teor. Fiz. 64, 1712 (1973) [Sov. Phys.-JETP 37, 864 (1973)].
[8]V. A. Gasparov, Zh. Eksp. Teor. Fiz. 68, 2259 (1975) [Sov. Phys.-JETP 41, 1129 (1976)]; and V. F. Gantmakher and V. A. Gasparov, Proceedings of the Fourteenth International Conference on Low Temperature Physics, (1975), Vol. 3, p. 52 (unpublished).
[9]M. R. Halse, Philos. Trans. R. Soc. 265, 507 (1969).
[10]P. B. Johnson, J. C. Kimball, and R. G. Goodrich, preceding paper, Phys. Rev. B 14, 3282 (1976).
[11]R. C. Jones, R. G. Goodrich, and L. M. Falicov, Phys. Rev. 174, 672 (1968).
[12]V. F. Gantmakher and E. A. Kaner, Zh. Eksp. Teor. Fiz. 45, 1930 (1963) [Sov. Phys.-JETP 18, 988 (1964)].
[13]J. M. Ziman, *Electrons and Phonons* (Oxford U. P., Oxford, 1963).
[14]D. K. Wagner and R. C. Albers, J. Low Temp. Phys. 20, 593 (1975).
[15]F. W. Young, Jr., and T. R. Wilson, Rev. Sci. Instrum. 32, 559 (1961).
[16]E. A. Faulkner and A. Holman, J. Sci. Instrum. 44, 391 (1967).
[17]J. C. Shaw, J. B. Ketterson, and L. R. Windmiller, Phys. Rev. B 5, 3896 (1972).
[18]D. G. Howard, Phys. Rev. 140, 1705 (1965).
[19]M. Springford, Adv. Phys. 20, 493 (1971).
[20]V. F. Gantmakher and V. A. Gasparov, Phys. Cond. Matter 19, 49 (1975).
[21]P. B. Johnson and R. G. Goodrich, J. Phys. F 6, L107 (1976).

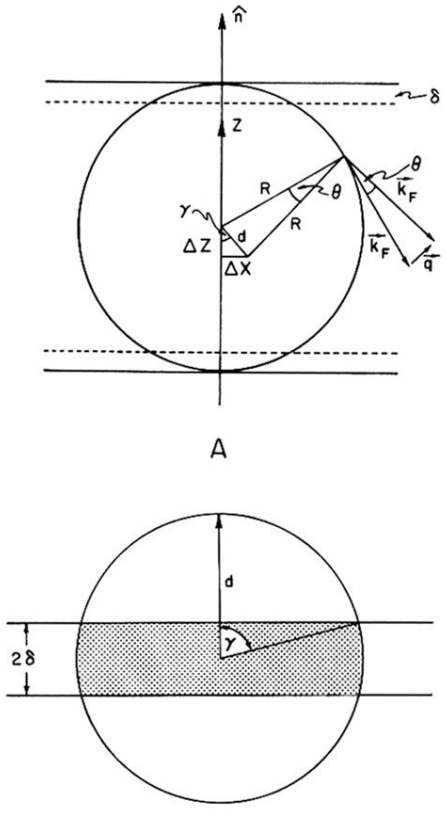

FIG. 2. (a) Result of a scattering event on a circular orbit in the RFSE geometry, where γ is the angle between the orbit center displacement and $\hat{n}$. (b) Locii of orbit centers produced by scatterings shown in (a) at different points on the orbit. The thickness of the shaded area is twice the skin depth, and the radius d is determined by the average scattering angle θ.